Current Research in Food Science 6 (2023) 100404

Contents lists available at ScienceDirect

Current Research in Food Science

journal homepage: www.sciencedirect.com/journal/current-research-in-food-science

An extrusion-based 3D food printing approach for generating alginate-pectin particles

Valentine Barbara J. Rysenaer [a,b], Safoura Ahmadzadeh [a], Filip Van Bockstaele [b], Ali Ubeyitogullari [a,c,*]

[a] Department of Food Science, University of Arkansas, Fayetteville, AR, 72704, USA
[b] Department of Food Technology, Safety and Health, Faculty of Bioscience Engineering, Ghent University, 9000, Ghent, Belgium
[c] Department of Biological and Agricultural Engineering, University of Arkansas, Fayetteville, AR, 72701, USA

ARTICLE INFO

Handling editor: Dr. Xing Chen

Keywords:
Extrusion
3D food printer
Alginate
Pectin
Hydrogel beads
Biopolymer
Delivery

ABSTRACT

In the present study, alginate-pectin (Al–P) hydrogel particles containing varied total gum concentrations (TGC) at a constant Al:P ratio of 80:20 were formed utilizing an innovative extrusion-based 3D food printing (3DFOODP) approach. The 3DFOODP conditions, namely, TGC (1.8, 2.0, and 2.2 wt%) and nozzle size (0.108, 0.159, and 0.210 mm) were investigated. The 3DFOODP approach was compared with the conventional bead formation method via a peristaltic pump. All Al–P printing inks exhibited a shear-thinning behavior. The increased apparent viscosity, loss and storage moduli were associated with the increase in the TGC. The size of the wet 3D-printed Al–P hydrogel particles ranged between 1.27 and 1.59 mm, which was smaller than that produced using the conventional method (1.44–1.79 mm). Freeze-dried Al–P particles showed a porous structure with reduced crystallinity. No chemical interaction was observed between alginate and pectin. This is the first report on generating Al–P-based beads using a 3DFOODP technique that can create delivery systems with high precision and flexibility.

1. Introduction

Through the combination of recent developments and its great potential, 3DFOODP technology has recruited considerable attention as a promising technique for assembling customized foods (Liu et al., 2020). 3DFOODP can precisely control not only the geometry but also the composition of foods, enabling the development of visually appealing and nutritionally customized foods. Due to its high flexibility, 3DFOODP has attracted great interest in developing personalized foods for several industries, such as military (Caulier et al., 2020) and deep space (Enfield et al., 2022; Le-Bail et al., 2020). Thus far, several 3D printing techniques, including selective laser sintering, extrusion-based printing, binder jetting, and inkjet printing, have been implemented for printing foods (Le-Bail et al., 2020; Lipton et al., 2015; Sun et al., 2015). Among these printing techniques, extrusion-based printing technology is currently the most widely utilized 3D printing technique for food manufacturing due to the large variety of suitable food inks, flexibility, and high printing speed (Liu et al., 2020). Currently, the extrusion-based 3D printing technique has been mainly used for printing macroscale (~cm scale) food objects from materials such as chocolate (Hao et al., 2010), cheese (Periard et al., 2007), and ground meat (Lipton et al., 2015). However, creating food microstructures for the delivery of micronutrients using 3DFOODP has not been fully explored yet (Ahmadzadeh and Ubeyitogullari, 2022a).

Hydrogels have been investigated as encapsulation media for nutrient and drug delivery in the food, biomedical, bioprocessing, and pharmaceutical industries (Guo and Kaletunç, 2016). For instance, hydrogels have been utilized for the targeted delivery of β-carotene (Guedes Silva et al., 2021), insulin–transferrin conjugates (Kavimandan et al., 2006), and antimicrobial peptides (Borro et al., 2020), where bioactive compounds are physically entrapped in the polymeric matrix of the hydrogel (Guo and Kaletunç, 2016; Lee et al., 2013). By isolating the bioactive compounds from the outer environment, encapsulant provides protection during food processing, storage, and gastric digestion (Guo and Kaletunç, 2016).

Among food-grade biopolymers generating hydrogels, alginate and pectin have received great attention due to their commercial availability, low cost, biocompatibility, and biodegradability. Specifically,

* Corresponding author. N205, 2650 N. Young Ave., Fayetteville, AR, 72704.
E-mail address: uali@uark.edu (A. Ubeyitogullari).

https://doi.org/10.1016/j.crfs.2022.11.023
Received 28 June 2022; Received in revised form 22 November 2022; Accepted 28 November 2022
Available online 2 December 2022

alginate is one of the most broadly utilized polymeric materials for creating hydrogels for encapsulation purposes. The molecular chain structure of alginate consists of linear binary copolymers, beta-D mannuronic acid (M block), and alpha-L glucuronic acid (G block), combined through 1,4 linkages (Lee et al., 2013). Pectin is another polysaccharide-based polymer that consists of D-galacturonic acid units joined in chains through alpha-1,4 glycosidic linkages with different degrees of methyl esters substituents (Auriemma et al., 2013). Similar to alginate, gel formation occurs through cross-linking between pectin and calcium ions (Jaya et al., 2009).

The pH-responsive characteristic of Al–P hydrogel particles distinguishes them from either alginate or pectin gels only since neither of them alone forms a gel upon decreasing the pH. The Al–P hydrogels are expected to go through a gel-solution transition as the pH rises (Guo and Kaletunç, 2016). Furthermore, alginate-pectin gels provide better encapsulation efficiency, protection, and release compared to those prepared with alginate or pectin alone (Guo et al., 2018; Guo and Kaletunç, 2016; Madziva et al., 2005). Therefore, there are numerous opportunities for alginate and pectin blends to be used in the delivery of pH-sensitive drugs/nutrients and microorganisms/cells (Guo and Kaletunç, 2016).

So far, alginate-pectin hydrogel particles have been manufactured using the conventional approach, which entails manufacturing the particles with a peristaltic pump. Although the resulting hydrogel particles generated using a peristaltic pump are generally effective, the flow rate is sensitive to altering differential pressure circumstances (Klespitz and Kovács, 2014). In addition, due to variances produced by manufacturing and tubing replacement, the pump system must be calibrated to obtain acceptable accuracy. In some circumstances, their chemical inertness can be a problem (Klespitz and Kovács, 2014). Thus, in this study, 3DFOODP has been employed for generating alginate-pectin hydrogel particles for the first time. The benefits of using the 3DFOODP over the traditional approach of Al–P hydrogel particle formation include high precision and flexibility, where high precision enables generating particles consistently with high accuracy, and high flexibility allows to develop different shapes/sizes with different material compositions for versatile applications (Ahmadzadeh and Ubeyitogullari, 2022b). For example, the 3DFOODP approach can provide fine control over the design and composition of the particles while enabling the use of various polymers at the same time in different cartridges. Bioactive compounds and live microorganisms/cells could be encapsulated in Al–P hydrogel particles using a 3DFOODP without damaging the microorganisms/cells during the printing process (Schaffner et al., 2017). 3D printing of alginate/pectin along with other biopolymers has been reported for tissue engineering applications (Agarwal et al., 2021; S. Hu et al., 2021; Nguyen et al., 2017; You et al., 2017). However, to the best of our knowledge, there is no report on forming alginate-pectin hydrogel particles using an extrusion-based 3DFOODP.

Therefore, the main objective of this study was to generate alginate-pectin particles using 3DFOODP technology. Specific objectives were to: (a) investigate the effects of 3D printing parameters, namely, TGC, nozzle size, and extrusion pressure on particle size and shape, (b) characterize the freeze-dried alginate-pectin particles for their size, morphology, crystallinity, and chemical structure, and (c) compare the particle sizes of alginate-pectin particles synthesized using traditional methods versus those produced using 3DFOODP.

2. Materials and methods

2.1. Materials

Pectin (AM 800) in powdered form was obtained from Ingredion (Westchester, IL). The degree of esterification (DE) of the pectin was 69–72%. Alginic acid sodium salt with medium viscosity (~3500 cps, 2% aqueous solution), was obtained from MP Biomedicals (Solon, OH). Calcium chloride ($CaCl_2$) with 97 wt% purity was purchased from Alfa Aesar (Haverhill, MA).

2.2. Preparation of alginate-pectin gel solution

Solutions of 1.75 and 2.0 wt% alginate, and 4.0 wt% pectin were prepared by dissolving the powders in deionized water using a magnetic stirrer at ambient temperature (23 °C) for 2.5 h following the methods described by Guo and Kaletunç (2016) and Belščak-Cvitanović et al. (2015). The different solutions were mixed in various ratios to obtain the appropriate TGC and Al–P weight percent ratio after being incubated at 4 °C for 8 h to permit air bubbles to rise. Al–P solutions of 1.6–3.0 wt% TGC were created for screening studies, with the Al–P weight ratio kept constant at 80:20.

2.3. Preparation of hydrogel particles via the conventional method

A peristaltic pump (Masterflex L/S, Cole Parmer, IL, USA) was used to generate Al–P hydrogel particles following the method of Guo and Kaletunç (2016). The Al–P solution was extruded through a 0.337 mm, 0.210 mm, 0.159 mm, and 0.108 mm inner diameter needles (Allevi, 3D Systems, Inc., PA, USA) at room temperature (23 °C) with a volumetric flow rate of 0.027 mL/s and a dropping distance of 2.5 or 5 cm, in order to obtain spherical particles. The nozzle size of 0.337 mm was selected for comparing the data with the literature (Guo and Kaletunç, 2016), while nozzle sizes of 0.210, 0.159, and 0.108 mm were used to compare this method with the 3DFOODP technique described below. The extruded droplets formed hydrogel particles as they interacted with the 0.1 M $CaCl_2$ curing solution for 3–4 h (Jaya et al., 2009; Lee et al., 2013).

2.4. Preparation of hydrogel particles using 3D food printing

The hydrogel particles were obtained via a droplet extrusion-based method using a 3D food printer (Allevi 2, 3D Systems, Inc., PA, USA) equipped with two 10-mL cartridges. The extrusion system was operated with pneumatic pressure (1–120 psi). The alginate-pectin solutions were loaded into one of the cartridges and extruded through 0.210 mm, 0.159 mm, and 0.108 mm inner diameter needles (Allevi, 3D Systems, Inc., PA, USA) at room temperature (23 °C). Extrusion height was adjusted to 2.5 or 5 cm, while the printing speed was kept constant at 6 mm/s. A stereolithography (stl) file of a sphere was selected using the Bioprint Pro software for releasing a known amount of the Al–P solution into the $CaCl_2$ solution. The extrusion time was 1 s for each hydrogel droplet, which was confirmed by estimating the average time required for printing 64 droplets. Table 1 lists the 3DFOODP conditions studied. The extruded droplets formed hydrogels as they interacted with the 0.1 M $CaCl_2$ solution. The particles were hardened in the $CaCl_2$ solution for 3–4 h (Jaya et al., 2009). Finally, they were washed thoroughly with deionized water to remove excess $CaCl_2$ ions from the hydrogel particles.

2.5. Rheological properties

The AR 1000-N Rheometer (TA Instruments, DE, USA), a controlled-stress rheometer equipped with a Peltier Plate temperature control

Table 1
3D printing conditions of alginate-pectin hydrogel particles.

Total gum concentration (wt.%)	Nozzle size (I.D. mm)	Extrusion pressure (psi)
1.8	0.210	18
	0.159	25
	0.108	50
2.0	0.210	23
	0.159	28
	0.108	54
2.2	0.210	27
	0.159	34
	0.108	60

device and a 40 mm parallel-plate geometry, was used to study rheological properties of Al–P solutions with varying total gum concentrations. The temperature was set at 25 °C, and the experimental gap was adjusted to 1.00 mm. The linear viscoelastic region (LVR) was identified via performing strain sweep tests at a frequency of 1 Hz following the methods described by Vicini et al. (2017) and M. Hu et al. (2020). For all experiments, the equilibration time was set to 5 min at 1 Hz with 0.01% strain falling within the LVR. The angular frequency was increased from 0.6 to 250 rad/s at 1 Pa for the angular frequency sweep test, and the elastic (G′) and viscous (G″) moduli were recorded.

2.6. Particle size analysis

The size of the particles was measured using ImageJ software (ImageJ 1.53k, National Institutes of Health, USA). Randomly selected 20 particles were used to determine the mean particle size. The particle size was measured for TGCs of 1.8, 2.0, and 2.2 wt%, with nozzle sizes of 0.337 mm, 0.210 mm, 0.159 mm, and 0.108 mm inner diameter for particles generated by the conventional method, and nozzle sizes of 0.210 mm, 0.159 mm, and 0.108 mm inner diameter for particles formed by the 3DFOODP. The size of the particles generated through a nozzle size of 0.337 mm inner diameter was investigated to compare the results with the study conducted by Guo and Kaletunç (2016).

2.7. Freeze-drying of the particles

The washed Al–P hydrogel particles were frozen at −80 °C for 3 h before being lyophilized (SP VirTis BenchTop SLC, SP scientific, NY, USA) for 2 days at a condenser temperature of −108 °C under vacuum pressure of 0.015 kPa. After drying, the beads were placed in a container that was immediately sealed for future use.

2.8. Density and porosity

The true density of the freeze-dried Al–P particles was measured using a gas displacement pycnometer system (AccuPyc II, Micromeritics Instrument Corporation, GA, USA), where helium was used as the displacement medium. The bulk density of the particles was determined by measuring their weight and volume. Then, the porosity (%) was determined using the true and bulk densities by the following equation:

$$\varepsilon = \left(1 - \frac{\rho_{bulk}}{\rho_{true}}\right) * 100 \quad (1)$$

2.9. Morphology of the dried particles

Scanning electron microscopy (SEM) micrographs of dry Al–P particles were generated using an FEI Nova Nanolab 200 Dual-Beam system equipped with a 30 kV SEM FEG column and a 30 kV FIB column following the method described by Ubeyitogullari and Ciftci (2016). Specimens were prepared by cutting thin cross-sections from the particles, which were subsequently sputter-coated with a thin gold layer using a sputter coater (EMITECH SC7620 Sputter Coater, MA, USA). SEM images were captured at an acceleration voltage of 15.0 kV, and an electric current of 10 mA.

2.10. X-ray diffraction

The X-ray diffraction patterns of the samples were recorded at ambient temperature (23 °C) using a PW3040 X'Pert MRD High-Resolution XRD (Philips, Almelo, Netherlands) following the method described by Jaya et al. (2009). Powdered particles were analyzed at two theta angles ranging from 5° to 55° at a voltage of 45 kV, an electric current of 40 mA, and with a scan step size of 0.02°. The same procedure was applied to analyze pure alginate and pectin. OriginPro 2021 (OriginLab Corporation, MA, USA) was used to calculate the crystallinity index by dividing the area under the crystalline peaks to the total area under the curve (i.e., both the amorphous region and the crystalline peaks) (Helmiyati and Aprilliza, 2017; Mishra et al., 2008).

2.11. Fourier transform infrared (FTIR) spectroscopy

An FTIR spectrometer (IRAffinity-1S, Shimadzu, Japan) equipped with a Quest attenuated total reflectance (ATR) was utilized to acquire the FTIR spectra of the freeze-dried Al–P particles with different TGC (i.e., 1.8, 2.0, and 2.2 wt%). The FTIR spectra were generated in the wavelength range of 400–4000 cm^{-1} at a resolution of 4 cm^{-1} with 64 scans.

2.12. Statistical analysis

The data were analyzed by R (Version 4.0.4., R Foundation for Statistical Computing, Vienna, Austria) using a one-way analysis of variance (ANOVA) with Tukey's multiple comparison test at a 95% confidence level. The hydrogel beads were produced in triplicates for each processing condition, where a new gel solution was formed for each replication. The results are presented as the mean value ± standard deviation.

3. Results and discussion

3.1. Preparation of the hydrogel particles

In this study, the droplet extrusion method was used to generate the Al–P hydrogel particles utilizing a peristaltic pump or a 3D food printer. Droplet extrusion is a manufacturing method wherein a biopolymer solution is extruded through a capillary and permitted to split away from the needle in droplet form affected by a gravitational force or external force into a curing solution (Lee et al., 2013). Although Al–P hydrogel particles were formed upon contacting the $CaCl_2$ solution in both systems, the traditional pump method had a constant flow of the polymer solution dripping into the $CaCl_2$ solution, whereas the 3DFOODP approach released a known amount of Al–P solution for each hydrogel particle, which was determined by the.stl file used in the printing software. The curing solution was 0.1 M $CaCl_2$ solution, a commonly used $CaCl_2$ concentration for bead manufacturing due to its effect on bead size, structure, and potential encapsulation applications (Lee et al., 2013). Even though high methoxyl pectins do not have enough affinity to Ca^{2+} to form a gel at pH 5–7, they can form strong gels at lower pHs (~3) in the presence of a solute (Tibbits et al., 1998). Therefore, Al–P composite polymers were used together to create the hydrogel particles that could provide extra protection in acidic environments such as the stomach. For example, in a previous study, Al–P hydrogel particles generated without Ca^{2+} ions stayed intact at pH 3.0 for 23 days (Guo and Kaletunç, 2016).

In the preliminary studies, hydrogel particles were prepared at eight TGCs (i.e., 1.6, 1.8, 2.0, 2.2, 2.4, 2.5, 2.7, and 3.0 wt%), and two drop heights (i.e., 2.5 and 5 cm). The capacity to produce particles with the smallest needle size (i.e., 0.108 mm) resulted in the exclusion of TGC greater than 2.2 wt%, due to the undesirable high pressure (i.e., pressures greater than 65 psi). On the other hand, due to the low viscosity properties, total gum concentrations less than 1.8 wt% were unable to form spherical particles using the 3DFOODP with the largest nozzle size (i.e., 0.210 mm), and therefore, they were excluded from the experimental plan. As a result, the TGC was set to be between 1.8 and 2.2 wt% for further hydrogel particle preparation and characterization. In addition, the drop height of 2.5 cm was eliminated as the produced particles with this drop height were not in a spherical shape. Consequently, all Al–P hydrogel particles were formed at a drop height of 5.0 cm.

3.2. Rheological properties

The apparent viscosity of the gel solutions, used as 3D printing inks, is expected to be low enough to permit easy extrusion through the nozzle tip, while yet being sufficiently high to allow the ink to be stacked with previously deposited layers (Liu et al., 2020). In extrusion-based 3D printing, the viscosity reduction caused by shear deformation is defined as shear-thinning behavior, which helps the ink to flow smoothly through a small deposition needle. However, the viscosity of the ink is recovered upon depositing, resulting in better shape integrity (Huang et al., 2021).

The apparent viscosities of the Al–P solutions as a function of shear rate are illustrated in Fig. 1a. The apparent viscosity increased with increasing the TGC. This is due to the alginate and pectin's tendency to form hydrogen bonds with water molecules, resulting in a denser network (Liu et al., 2020). Hydrocolloids form strong structures by water removal from the system. Also, as reported by Sokolovska et al. (2016), hydrogen bonds formed between chains of sodium alginate and pectin in combined systems increase the portion of bound water. Therefore, in this study, free water has decreased by increasing the TGC, resulting in a stronger network and higher viscosity (Sokolovska et al., 2016).

All the Al–P solutions exhibited shear-thinning behavior, associated with gradually decreased apparent viscosity with increasing shear rate, and suggested that all pastes were non-Newtonian fluids, which is critical to achieving a successful 3D printing. These findings are consistent with the prior research conducted by Liu et al. (2020) and Gómez-Dí;az and Navaza (2003), who found that increasing sodium alginate concentration leads to higher apparent viscosity.

The mechanical spectrum of a material can be represented as a variation of G′ and G″ with angular frequency. The solid-like behavior (G′) dominates the liquid-like, viscous characteristics (G″) in a typical mechanical spectrum of polysaccharide solutions and gels (Moreira et al., 2014). The strength of the gel formed between alginate and pectin is associated with their chemical structure. With an increase in DE, methyl groups on the pectin chain reduce the electrostatic repulsions, leading to a better molecular association and the formation of stronger gels (Walkenström et al., 2003). In the present study, high methoxyl pectin (DE: 69–72%) was used with alginate, generating hydrogels with appropriate printability.

Fig. 1b and c illustrates the logarithmic representation of the G′, and G″, respectively, as a function of the angular frequency, revealing the characteristic spectrum of a hydrogel. The highest absolute values of both G′ and G″ were observed in the hydrogel solution with the highest TGC. In addition, G′ was higher than G″ for all the samples, confirming the dominant solid-like behavior. However, the almost parallel increase in G' and G" curves with the increase in the angular frequency reveals a weak Al–P gel formed (Ye et al., 2021). This was further investigated by determining the loss tangent (tan $\delta = G''/G'$) (Fig. 1d). Tan δ gives information about the relative mechanical strength of the gel solutions, where tan $\delta < 0.1$ indicates strong, self-standing gels while $1 > \tan\delta > 0.1$ reveals weak, paste-like gels, and tan $\delta > 1$ shows a liquid-like behavior (Hazur et al., 2020; Koo et al., 2014). The tan δ values for all solutions investigated, lied between the range of $1 > \tan\delta > 0.1$, indicating an overall paste-like gel behavior. Previously, Hazur et al. (2020) reported tan δ values greater than 1 for alginate solutions (2 wt%), while Koo et al. (2014) reported tan δ lower than 1 for alginate solutions (1.5 wt%) with Tween-80 (0.2 wt%), xanthan gum (0.2 wt%), and glycerol (5 wt%). These differences can be explained by the nature of the sodium alginate used (i.e., low viscosity, < 300 cps; medium viscosity, ~3500 cps; or high viscosity, ~ 14000 cps).

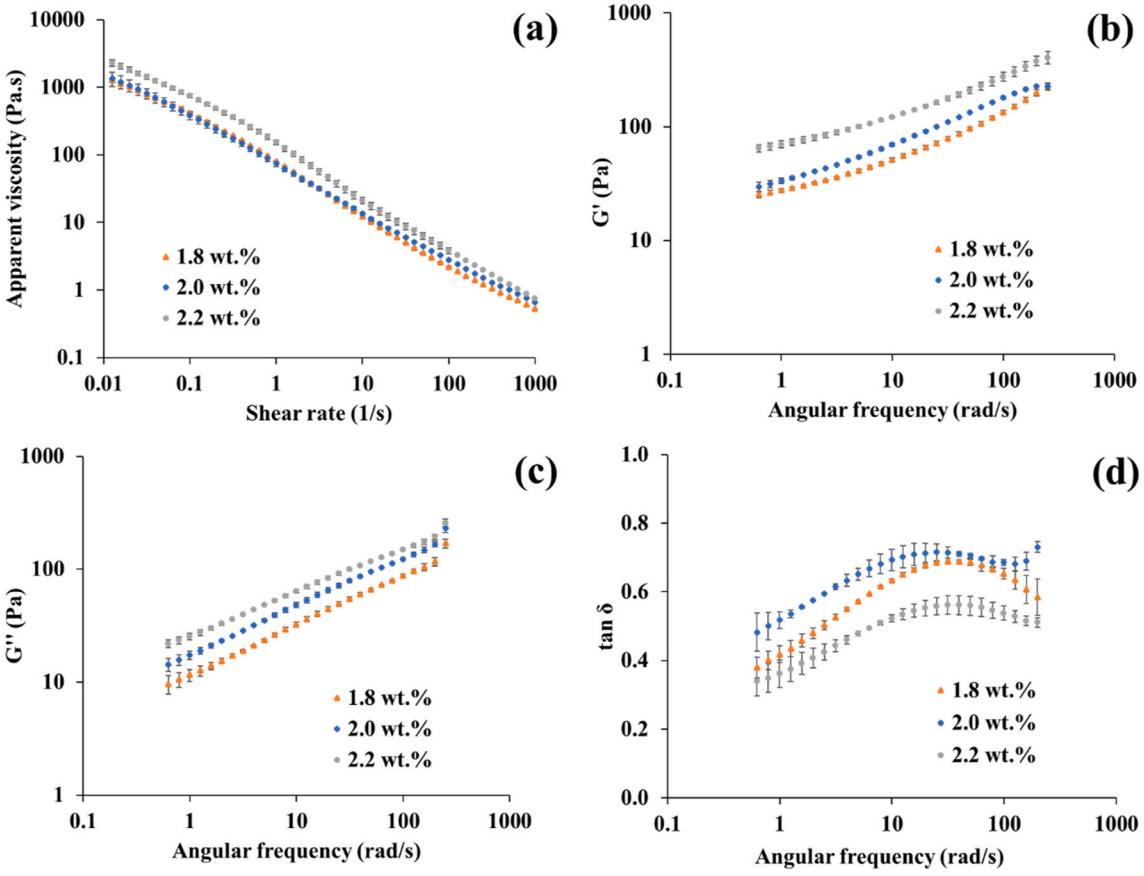

Fig. 1. (A) Viscosity as a function of shear rate at 25 °C; (b) G'; (c) G"; and (d) tan δ as a function of angular frequency for Al–P solutions at various concentrations.

3.3. Particle size

Fig. 2 shows the average particle size of the wet Al–P hydrogel particles generated via the conventional method (Fig. 2a), as well as produced utilizing the 3DFOODP (Fig. 2b). All the generated Al–P hydrogel beads were in a spherical shape (Fig. 3). The particle size of the Al–P hydrogel beads varied between 1.44 and 1.79 mm when the peristaltic pump was used with different nozzle sizes (0.108–0.210 mm) and TGC (1.8–2.2 wt%) (Fig. 2a). On the other hand, 3DFOODP created particles in the range of 1.27–1.59 mm (Fig. 2b). When the particles were created using the peristaltic pump rather than the 3DFOODP under identical conditions, such as using the same nozzle size and TGC, the particles produced were significantly larger ($p < 0.05$). For example, the Al–P hydrogel particles generated via 3DFOODP using a TGC of 1.8 wt% with a nozzle size of 0.108 mm had a particle size of 1.27 mm, whereas the Al–P hydrogel particles produced using the peristaltic pump at the same conditions resulted in significantly larger particle size of 1.44 mm ($p < 0.05$) (Fig. 2). Compared to the particles produced with 3DFOODP, the particles created with the peristaltic pump showed larger variation in their size; specifically, the standard deviation was approximately 39.5% greater. Furthermore, using the peristaltic pump with the smallest nozzle size (0.108 mm) and the highest TGC (2.2 wt%) resulted in no particle formation due to the pressure build-up in the system.

As the TGC increased from 1.8 to 2.2 wt%, the hydrogel particle size significantly increased for both systems (i.e., 3DFOODP and peristaltic pump), especially with larger nozzle sizes (e.g., 0.210 and 0.159 mm). This can be due to the increase in the viscosity of Al–P solutions as the TGC was increased (Fig. 1a). Specifically, as the viscosity of the Al–P solutions increases, it is more difficult for the particles to separate from the tip of the nozzle (F. Chen et al., 2018). Furthermore, the particle size of Al–P hydrogel beads decreased with decreasing the nozzle size as expected (Fig. 2). The smallest Al–P particles (1.27 mm) were obtained via 3DFOODP with the smallest nozzle size (0.108 mm) and lowest TGC (1.8 wt%). However, the particle size only slightly increased to 1.30 and 1.34 mm ($p > 0.05$) when the TGC increased to 2.0 or 2.2 wt% at these conditions (Fig. 2b). These findings are consistent with those of Davarcı et al. (2017), where smaller calcium alginate beads were obtained with smaller nozzle sizes (~0.7–1.8 mm OD) and lower alginate concentrations (1.0–3.0 wt%).

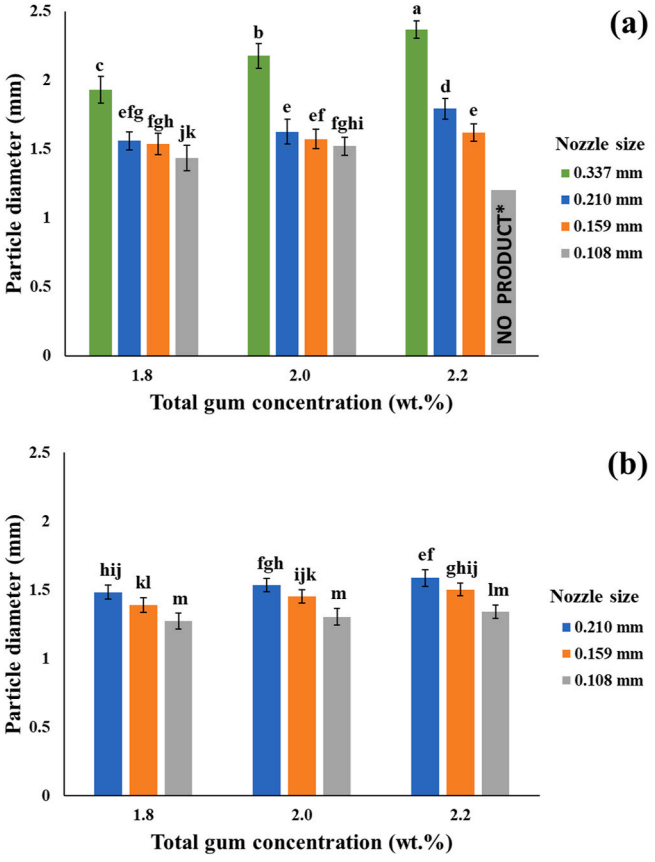

Fig. 2. The particle size of Al–P hydrogels generated via (a) the conventional and (b) 3D food printing methods. *NO PRODUCT means it was not possible to form droplets from 2.2 wt% TGC using the nozzle size of 0.108 mm inner diameter. The nozzle size of 0.337 mm was used for comparison with the literature. Different letters above data points indicate that they are significantly different ($p < 0.05$).

Guo and Kaletunç (2016) obtained spherical Al–P particles utilizing a peristaltic pump where the particles were produced using a 2.2 wt% TGC (82:18 alginate:pectin ratio) gel solution with a 0.337 mm nozzle size at 5 cm drop height. The Al–P particles generated at these conditions had a particle diameter of 2.68 mm (Guo and Kaletunç, 2016). Using the identical needle size, equipment, TGC, and drop height, spherical particles with an average diameter of 2.37 mm were created in this study. The different alginate:pectin ratio (80:20 vs. 82:18), curing solution (0.1 M $CaCl_2$ vs. 0.1 M pH 1.2 HCl/KCl buffer), and volumetric flow rate (0.027 vs. 0.017–0.022 mL/s) could explain the variation in the particle sizes. These differences in alginate:pectin ratio, curing solution, and volumetric flow rate were due to following a different method to prepare the solutions (Belščak-Cvitanović et al., 2015), more practical applications with 3DFOODP, and peristaltic pump limitations, respectively. Furthermore, a study conducted by Kiaei Pour et al. (2020) obtained Al–P hydrogel particles with a particle size of 4.10 mm using a 1.8 wt% TGC and 80:20 alginate:pectin ratio. The microcapsules were prepared using a syringe pump by dripping the Al–P solution into a 1 M $CaCl_2$ solution through a 0.6 mm syringe needle at a flow rate of 1.0 mL/min. Similarly, Al–P particles with an average size of 2.11 mm were obtained by Belščak-Cvitanović et al. (2015). The particles were formed using an Al–P solution with a 2.0 wt% TGC and 80:20 alginate:pectin ratio utilizing a 5 mL syringe with a 0.337 mm nozzle size. In this study, using the peristaltic pump with the identical needle size, alginate:pectin ratio, and TGC, Al–P particles with a size of 2.03 mm were generated. The small difference in the particle size could be explained by the varied equipment (peristaltic vs. syringe pump) and curing solution (0.1 M $CaCl_2$ vs. ~0.2 M $CaCl_2$).

3.4. Particle size, density, and porosity of the freeze-dried Al–P particles

After comparing the Al–P bead formation techniques (i.e., the conventional vs. 3DFOODP), only the 3D-printed Al–P hydrogel particles were freeze-dried and characterized further since it was not expected to observe differences due to the bead production methods. However, the 3D-printed Al–P particles were characterized in detail due to the limited data (e.g., SEM, FTIR, and XRD data) on alginate and high methoxyl pectin particles in the literature and in order to facilitate the potential applications of these particles in the food and pharmaceutical industries.

Freeze-drying was employed as a drying method to relatively preserve the hydrogel structure and form interconnected porous Al–P polymers. After freeze-drying, the generated Al–P particles were characterized for their size, density, and porosity (Table 2). All the particles were generated using a nozzle size of 0.159 mm. The sizes of the freeze-dried Al–P particles formed using TGCs of 1.8, 2.0, and 2.2 wt% were 1.08, 1.18, and 1.27 mm, respectively. Compared to their sizes before freeze-drying (Fig. 2b), Al–P hydrogels with higher TGC resulted in less shrinkage. At higher TGC, more Al–P molecules were present in the same volumetric area, supporting the structure to minimize shrinkage during drying (Bera et al., 2015; M. Hu et al., 2020). This also led to a lower bulk density and a higher porosity at the TGC of 2.2 wt% (Table 2), where the true density of the Al–P particles was measured as 1.86 ± 0.02 g/cm^3.

Gelation of the Al–P solutions starts as the biopolymers come into

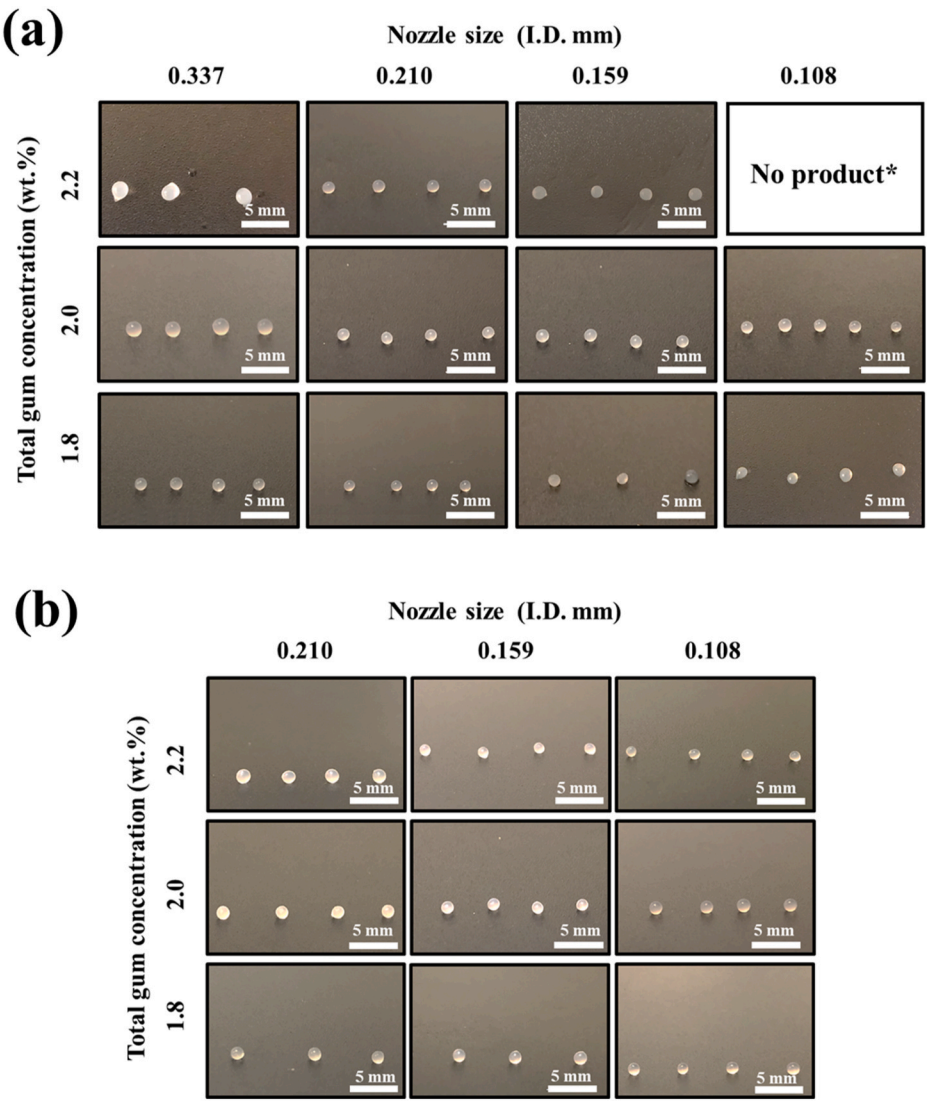

Fig. 3. Pictures of Al–P hydrogel particles generated using (a) the conventional and (b) 3D food printing methods. *No product means it was not possible to form droplets from 2.2 wt% TGC using the nozzle size of 0.108 mm inner diameter via the conventional method.

Table 2
Particle diameter, bulk density, and porosity of freeze-dried Al–P particles.

Total gum concentration (wt.%)	Particle diameter (mm)	Bulk density (g/cm^3)	Porosity (%)
1.8	1.08 ± 0.03^a	0.09 ± 0.01^a	95.1 ± 0.3^b
2.0	1.18 ± 0.07^a	0.06 ± 0.01^b	96.7 ± 0.1^a
2.2	1.27 ± 0.13^a	0.06 ± 0.01^b	97.2 ± 0.5^a

* All the particles were formed using a 3D food printing system with a nozzle size of 0.159 mm at extrusion pressures of 25, 28, and 34 psi for TGC of 1.8, 2.0, and 2.2 wt%, respectively. Data are given as means of triplicates ± standard deviations. Values in the same column with different superscript letters are significantly different ($p < 0.05$).

contact with the $CaCl_2$ solution. The gelation starts from the surface of the droplet, and as $CaCl_2$ diffuses into the droplet, the biopolymers at the center of the droplet cross-links with Ca^{2+} ions (M. Hu et al., 2020). Therefore, since the diffusion of Ca^{2+} into the droplets generated with a lower TGC is faster owing to their lower viscosity (Fig. 1a), these droplets are expected to have a higher cross-linking density compared to that of formed with a higher TGC. Consequently, the higher number of Ca^{2+} present in the structure of Al–P particles formed with a lower TGC may have also contributed to their increased density (Table 2). In general, high-porosity particles could be useful as microencapsulation carriers for bioactive compounds (K. Chen and Zhang, 2019).

3.5. Morphology of the freeze-dried Al–P particles

The morphology of the freeze-dried Al–P hydrogel particles at various TGCs was investigated using SEM (Fig. 4). All the samples showed a porous structure with irregular macropores where the pores were interconnected due to cross-linking of the polymers and ionic gelation. Ayarza et al. (2017) reported that the ionically cross-linked alginate beads indicate interconnected networks with high porosity compared to the alginic acid beads due to the fact that hydrogen bonding formed between chains in alginic acid beads are weaker than ionic cross-linking of the polymer.

In addition, the formation of ice crystals during freezing and then lyophilization of the beads also resulted in the generation of a macroporous structure (Stachowiak et al., 2021). SEM images revealed that the morphology of the particles slightly differed depending on the TGC. As the TGC increased, a more porous structure was observed, which can

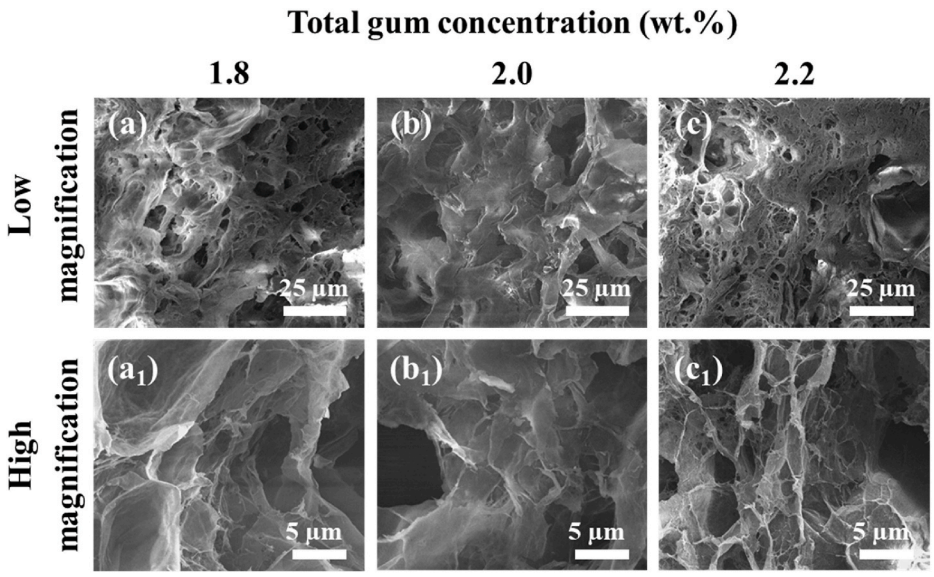

Fig. 4. SEM images of freeze-dried Al–P particles. All the particles were formed using a 3D food printing system with a nozzle size of 0.159 mm.

be due to the less shrinkage and collapsing of the particles caused by ionic cross-linking and freeze-drying, respectively (Fig. 4a_1,b_1,c_1). Also, at higher TGC, a denser hydrocolloid network structure increased gel stability against the growth of ice crystals. This result supports the density and porosity data obtained in this study (Table 2). Similar SEM images were reported by K. Chen and Zhang (2019) for freeze-dried Al–P particles produced using a 75:25 alginate:pectin ratio and 4 wt% TGC. Jaya et al. (2009) reported similar interconnected porous structures for Al–P microcapsules produced via the sol-gel method using $CaCl_2$ as the curing solution. The authors also reported the suitability of these structures for drug delivery systems.

3.6. X-ray diffraction

The X-ray diffraction patterns of the dried Al–P hydrogel particles with various TGC (i.e., 1.8, 2.0, and 2.2 wt%), pure alginate, and pectin are depicted in Fig. 5. Pectin showed diffraction peaks at $2\theta = 11.65°$, 13.05°, 14.25°, 18.8°, 19.50°, 22.50°, 24.75°, 38.4°, 46.1°, and 48.00°, respectively (Fig. 5a) while pure alginate exhibited a characteristic diffraction peak at $2\theta = 14.25°$ (Fig. 5b). Similar diffraction peaks have been reported for high-methoxyl pectin (Bera and Kumar, 2018) and alginate (L. Li et al., 2007). Freeze-dried Al–P particles had a single clear

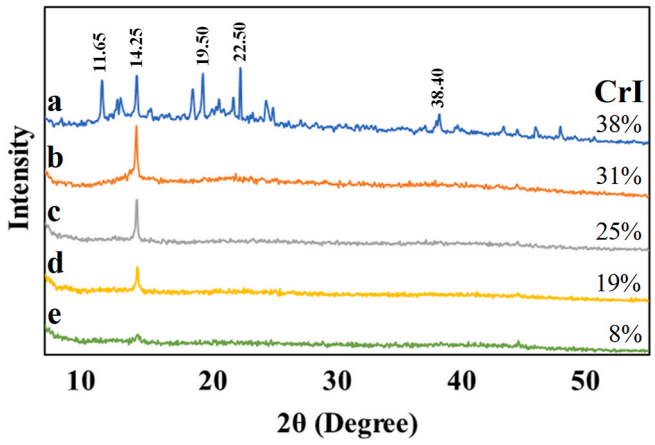

Fig. 5. XRD patterns of the (a) pectin, (b) alginate, and 3D-printed Al–P particles produced using TGC of (c) 1.8, (d) 2.0, and (e) 2.2 wt%. (CrI: Crystallinity index).

diffraction peak at $2\theta = 14.25°$, which was due to their alginate content and cross-linking with $CaCl_2$ and the resulting lateral packing among the molecules (L. Li et al., 2007). Characteristic peaks of pectin were not observed in the XRD patterns of Al–P particles in part due to its relatively low concentration. Also, the presence of Ca^{2+} could have disrupted pectin's inter-and intramolecular interactions, resulting in reduced crystallinity (Yang et al., 2018). Similarly, the loss of crystallinity in the XRD patterns of the Al–P particles can be explained by the ionic interactions between biopolymers damaging the crystalline configuration (Kiaei Pour et al., 2020). However, as the TGC increased, the intensity of the characteristic diffraction peak at $2\theta = 14.25°$ decreased (Fig. 5c,d,e). The Al–P particles' crystallinity indexes were also calculated (Fig. 5). The results showed that the crystallinity of the Al–P particles decreased as the TGC increased. The crystallinity indexes of sodium alginate (31%) and pectin (38%) were slightly different than the values reported in the literature (29% for sodium alginate (Helmiyati and Aprilliza, 2017) and 43% for pectin (Mishra et al., 2008)), which could be due to the source of the biopolymers, molecular weight (e.g., low vs. high viscosity sodium alginate), and degree of esterification (e.g., low vs. high methoxyl pectin). A study conducted by Cho et al. (2014) reported that the intensity of the peak at 2θ ~13° is associated with the number of lateral cross-linking. As described in Section 3.4., Al–P particles with a lower TGC are expected to have a higher cross-linking density, resulting in a more organized structure. Thus, the higher concentration of Ca^{2+} ions in the structure of Al–P particles formed with a lower TGC resulted in a higher peak intensity at $2\theta = 14.25°$, agreeing with the findings of Laia et al. (2014) and Prasetyaningrum et al. (2021).

3.7. Fourier transform infrared spectroscopy

Fig. 6 depicts the ATR-FTIR spectra of pectin, alginate, and the freeze-dried Al–P particles with various TGC in the wavenumber range of 4000–400 cm^{-1}. The FTIR spectra demonstrate the characteristic absorption peaks of the utilized ingredients for the particle formation (Fig. 6a and b), and the potential molecular interaction between alginate and pectin (Fig. 6c,d,e). The FTIR spectra of pure alginate showed absorption bands at 1591 and 1420 cm^{-1}, which correspond to asymmetric and symmetric stretching vibrations of carboxylate salt ion, respectively (Q. Li et al., 2021), and are specific to ionic bonding (Saarai et al., 2013). The absorption band related to C–O stretching was observed in the FTIR spectrum of pectin at the wavenumber of 1619 cm^{-1} (Jaya et al., 2009). The addition of pectin caused the formation of a new peak in the FTIR

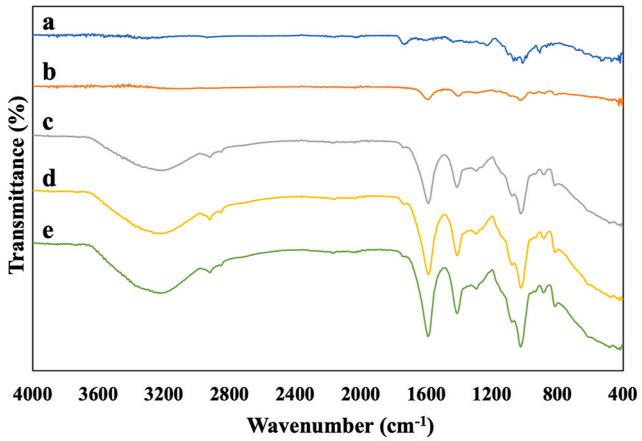

Fig. 6. ATR-FTIR spectra of the (a) pectin, (b) alginate, and 3D-printed Al–P particles produced using TGC of (c) 1.8, (d) 2.0, and (e) 2.2 wt%.

spectra of Al–P particles (1732 cm^{-1}) attributed to the C–O stretching in the carboxyl group (Kiaei Pour et al., 2020).

The FTIR spectra of the dried Al–P particles with different TGC (i.e., 1.8, 2.0, and 2.2 wt%) were similar (Fig. 6c,d,e). The absorption bands present in the FTIR spectra at 3700–3000 cm^{-1} and 3000–2850 cm^{-1} were attributed to O–H and C–H stretching vibrations, respectively (Vaziri et al., 2018). Similar FTIR spectra of alginate-pectin dried hydrogel beads are reported by Kiaei Pour et al. (2020).

For Al–P particles (TGC: 1.8, 2.0, 2.2 wt%), the carboxyl group characteristic peak at 1591 cm^{-1} shifted to 1597, 1589, and 1589 cm^{-1}, respectively, suggesting the cross-linking of sodium alginate with Ca^{2+}, agreeing with the results obtained by Badita et al. (2020) who reported the effect of ionic cross-linking on shifting in FTIR band corresponding to the carboxyl group. Compared to pure alginate, Ca^{2+} cross-linking resulted in an increase in the stretching carboxyl group (Vaziri et al., 2018). However, Badita et al. (2020) reported a reduction in the intensity of the carboxyl group characteristic peak when using a high concentration of Ca^{2+} for alginate gelation, which can explain the obtained results in the present study. Moreover, the shoulder that appeared at 1076 cm^{-1} was ascribed to the C–C and C–O stretching, which can also be related to the presence of ionic cross-linking. In another research conducted by Makaremi et al. (2019) on cross-linked films of Al–P, authors reported that shifting of COO^{-} characteristic peak could also be related to the powerful hydrogen bonding formed between two polymers. Overall, it is well studied that pectin and alginate are ionic polysaccharides, and they form hydrogels through chain-chain association, which is induced by the addition of divalent cations. As previously reported in the literature (da Silva et al., 2009), the specific interactions of calcium ions with guluronate in alginate and galacturonate in pectin resulted in gel formation.

Finally, no chemical interactions were observed between alginate and pectin (Fig. 6). Specifically, the FTIR spectra of the Al–P particles did not show any covalent bonds between alginate and pectin since the absorption bonds wavenumbers of the carboxylic group of alginate and the carbonyl group of pectin remained unaltered. These findings are consistent with the literature (da Silva et al., 2009), as those studies did not report the formation of new covalent bonds between alginate and pectin during gel formation.

4. Conclusions

Alginate-pectin hydrogel particles were successfully prepared by droplet extrusion using a 3DFOODP approach. In this study, the effects of Al–P TGC, nozzle size, and extrusion pressure on 3DFOODP were investigated, and the printing conditions were determined for creating small particle sizes. The 3DFOODP approach resulted in smaller Al–P particles compared to the conventional method using a peristaltic pump when similar conditions were used. All Al–P solutions showed a shear-thinning behavior, where their viscosity, loss and storage moduli increased with increasing the TGC. Generally, decreasing the TGC or the nozzle size resulted in a decrease in the particle size. The smallest particle size (1.27 mm) was achieved via 3DFOODP at a TCG of 1.8 wt% and a nozzle size of 0.108 mm. When the peristaltic pump was used, no particles were formed with the highest TGC (2.2 wt%) and the smallest nozzle size (0.108 mm), confirming the limitations of the conventional method and its low flexibility in generating particles compared to the 3DFOODP approach. All freeze-dried Al–P particles revealed an interconnected porous structure. TGC affected the ionic cross-linking with Ca^{2+} ions and also the shrinkage rate upon freeze-drying. The crystallinity of the freeze-dried Al–P particles was reduced compared to that of pure alginate and pectin. However, their crystallinity increased with the increased cross-linking density. FTIR spectra showed the ionic cross-linking with the Ca^{2+} ions; nevertheless, there was no indication of any chemical interaction between alginate and pectin, suggesting a physical entrapment of biopolymers. Overall, 3DFOODP has the potential to create Al–P particles with precise control over shape, size, and composition for developing delivery systems.

CRediT authorship contribution statement

Valentine Barbara J. Rysenaer: Conceptualization, Methodology, Validation, Investigation, Writing – original draft, Visualization. **Safoura Ahmadzadeh:** Conceptualization, Methodology, Investigation, Writing – review & editing. **Filip Van Bockstaele:** Conceptualization, Writing – review & editing, Supervision. **Ali Ubeyitogullari:** Conceptualization, Methodology, Validation, Visualization, Writing – review & editing, Supervision, Project administration, Funding acquisition, Resources.

Declaration of competing interest

The authors declare that they have no known competing financial interests or personal relationships that could have appeared to influence the work reported in this paper.

Data availability

No data was used for the research described in the article.

Acknowledgements

The authors gratefully acknowledge the financial support by the Research Incentive Grant (RIG) from the Arkansas Agricultural Experiment Station (AAES), Arkansas Biosciences Institute (ABI), and also the USDA National Institute of Food and Agriculture, Multistate Project NC1023, Accession number 1025907.

References

Agarwal, T., Costantini, M., Maiti, T.K., 2021. Extrusion 3D printing with pectin-based ink formulations: recent trends in tissue engineering and food manufacturing. Adv. Biomed. Eng. 2, 100018 https://doi.org/10.1016/j.bea.2021.100018.

Ahmadzadeh, S., Ubeyitogullari, A., 2022a. Fabrication of porous spherical beads from corn starch by using a 3D food printing system. Foods 11 (7). https://doi.org/10.3390/foods11070913.

Ahmadzadeh, S., Ubeyitogullari, A., 2022b. Generation of porous starch beads via a 3D food printer: the effects of amylose content and drying technique. Carbohydr. Polym. 301, 120296 https://doi.org/10.1016/j.carbpol.2022.120296.

Auriemma, G., Mencherini, T., Russo, P., Stigliani, M., Aquino, R.P., Del Gaudio, P., 2013. Prilling for the development of multi-particulate colon drug delivery systems: pectin vs. pectin–alginate beads. Carbohydr. Polym. 92 (1), 367–373. https://doi.org/10.1016/j.carbpol.2012.09.056.

Ayarza, J., Coello, Y., Nakamatsu, J., 2017. SEM–EDS study of ionically cross-linked alginate and alginic acid bead formation. Int. J. Polym. Anal. Char. 22 (1), 1–10. https://doi.org/10.1080/1023666X.2016.1219834.

Badita, C.R., Aranghel, D., Burducea, C., Mereu, P., 2020. Characterization of sodium alginate based films. Rom. J. Phys. 65, 602.
Belščak-Cvitanović, A., Komes, D., Karlović, S., Djaković, S., Špoljarić, I., Mršić, G., Ježek, D., 2015. Improving the controlled delivery formulations of caffeine in alginate hydrogel beads combined with pectin, carrageenan, chitosan and psyllium. Food Chem. 167, 378–386. https://doi.org/10.1016/j.foodchem.2014.07.011.
Bera, H., Boddupalli, S., Nandikonda, S., Kumar, S., Nayak, A.K., 2015. Alginate gel-coated oil-entrapped alginate–tamarind gum–magnesium stearate buoyant beads of risperidone. Int. J. Biol. Macromol. 78, 102–111. https://doi.org/10.1016/j.ijbiomac.2015.04.001.
Bera, H., Kumar, S., 2018. Diethanolamine-modified pectin based core-shell composites as dual working gastroretentive drug-cargo. Int. J. Biol. Macromol. 108, 1053–1062. https://doi.org/10.1016/j.ijbiomac.2017.11.019.
Borro, B.C., Nordström, R., Malmsten, M., 2020. Microgels and hydrogels as delivery systems for antimicrobial peptides. Colloids Surf., B 187, 110835. https://doi.org/10.1016/j.colsurfb.2020.110835.
Caulier, S., Doets, E., Noort, M., 2020. An exploratory consumer study of 3D printed food perception in a real-life military setting. Food Qual. Prefer. 86, 104001 https://doi.org/10.1016/j.foodqual.2020.104001.
Chen, F., Zhang, Z., Deng, Z., Zhang, R., Fan, G., Ma, D., McClements, D.J., 2018. Controlled-release of antacids from biopolymer microgels under simulated gastric conditions: impact of bead dimensions, pore size, and alginate/pectin ratio. Food Res. Int. 106, 745–751. https://doi.org/10.1016/j.foodres.2018.01.038.
Chen, K., Zhang, H., 2019. Alginate/pectin aerogel microspheres for controlled release of proanthocyanidins. Int. J. Biol. Macromol. 136, 936–943. https://doi.org/10.1016/j.ijbiomac.2019.06.138.
Cho, A.R., Chun, Y.G., Kim, B.K., Park, D.J., 2014. Preparation of alginate–CaCl2 microspheres as resveratrol carriers. J. Mater. Sci. 49 (13), 4612–4619. https://doi.org/10.1007/s10853-014-8163-x.
da Silva, M.A., Bierhalz, A.C.K., Kieckbusch, T.G., 2009. Alginate and pectin composite films crosslinked with Ca2+ ions: effect of the plasticizer concentration. Carbohydr. Polym. 77 (4), 736–742. https://doi.org/10.1016/j.carbpol.2009.02.014.
Davarcı, F., Turan, D., Ozcelik, B., Poncelet, D., 2017. The influence of solution viscosities and surface tension on calcium-alginate microbead formation using dripping technique. Food Hydrocolloids 62, 119–127.
Enfield, R.E., Pandya, J.K., Lu, J., McClements, D.J., Kinchla, A.J., 2022. The future of 3D food printing: opportunities for space applications. Crit. Rev. Food Sci. Nutr. 1–14. https://doi.org/10.1080/10408398.2022.2077299.
Gómez-Díaz, D., Navaza, J.M., 2003. Rheology of aqueous solutions of food additives: effect of concentration, temperature and blending. J. Food Eng. 56 (4), 387–392. https://doi.org/10.1016/S0260-8774(02)00211-X.
Guedes Silva, K.C., Feltre, G., Dupas Hubinger, M., Kawazoe Sato, A.C., 2021. Protection and targeted delivery of β-carotene by starch-alginate-gelatin emulsion-filled hydrogels. J. Food Eng. 290, 110205 https://doi.org/10.1016/j.jfoodeng.2020.110205.
Guo, J., Giusti, M.M., Kaletunç, G., 2018. Encapsulation of purple corn and blueberry extracts in alginate-pectin hydrogel particles: impact of processing and storage parameters on encapsulation efficiency. Food Res. Int. 107, 414–422. https://doi.org/10.1016/j.foodres.2018.02.035.
Guo, J., Kaletunç, G., 2016. Dissolution kinetics of pH responsive alginate-pectin hydrogel particles. Food Res. Int. 88, 129–139. https://doi.org/10.1016/j.foodres.2016.05.020.
Hao, L., Mellor, S., Seaman, O., Henderson, J., Sewell, N., Sloan, M., 2010. Material characterisation and process development for chocolate additive layer manufacturing. Virtual Phys. Prototyp. 5 (2), 57–64. https://doi.org/10.1080/17452751003753212.
Hazur, J., Detsch, R., Karakaya, E., Kaschta, J., Teßmar, J., Schneidereit, D., Boccaccini, A.R., 2020. Improving alginate printability for biofabrication: establishment of a universal and homogeneous pre-crosslinking technique. Biofabrication 12 (4), 045004. https://doi.org/10.1088/1758-5090/ab98e5.
Helmiyati, Aprilliza, M., 2017. Characterization and properties of sodium alginate from brown algae used as an ecofriendly superabsorbent. IOP Conf. Ser. Mater. Sci. Eng. 188 (1), 012019 https://doi.org/10.1088/1757-899X/188/1/012019.
Hu, M., Zheng, G., Zhao, D., Yu, W., 2020. Characterization of the structure and diffusion behavior of calcium alginate gel beads. J. Appl. Polym. Sci. 137 (31), 48923 https://doi.org/10.1002/app.48923.
Hu, S., Martinez-Garcia, F.D., Moeun, B.N., Burgess, J.K., Harmsen, M.C., Hoesli, C., de Vos, P., 2021. An immune regulatory 3D-printed alginate-pectin construct for immunoisolation of insulin producing β-cells. Mater. Sci. Eng. C. 123, 112009 https://doi.org/10.1016/j.msec.2021.112009.
Huang, H., Ayariga, J., Ning, H., Nyairo, E., Dean, D., 2021. Freeze-printing of pectin/alginate scaffolds with high resolution, overhang structures and interconnected porous network. Addit. Manuf. 46, 102120 https://doi.org/10.1016/j.addma.2021.102120.
Jaya, S., Durance, T.D., Wang, R., 2009. Effect of alginate-pectin composition on drug release characteristics of microcapsules. J. Microencapsul. 26 (2), 143–153. https://doi.org/10.1080/02652040802211345.
Kavimandan, N.J., Losi, E., Peppas, N.A., 2006. Novel delivery system based on complexation hydrogels as delivery vehicles for insulin–transferrin conjugates. Biomaterials 27 (20), 3846–3854. https://doi.org/10.1016/j.biomaterials.2006.02.026.
Kiaei Pour, P., Alemzadeh, I., Vaziri, A.S., Beiroti, A., 2020. Potential effects of alginate–pectin biocomposite on the release of folic acid and their physicochemical characteristics. J. Food Sci. Technol. 57 (9), 3363–3370. https://doi.org/10.1007/s13197-020-04369-7.
23-25 Jan. 2014 Klespitz, J., Kovács, L., 2014. Peristaltic pumps — a review on working and control possibilities, Paper presented at the 2014. In: IEEE 12th International Symposium on Applied Machine Intelligence and Informatics (Sami).
Koo, S.Y., Cha, K.H., Song, D.-G., Chung, D., Pan, C.-H., 2014. Microencapsulation of peppermint oil in an alginate–pectin matrix using a coaxial electrospray system. Int. J. Food Sci. Technol. 49 (3), 733–739. https://doi.org/10.1111/ijfs.12358.
Laia, A.G. S.d., Costa Junior, E.d.S., Costa, H.d.S., 2014. A study of sodium alginate and calcium chloride interaction through films for intervertebral disc regeneration uses. Paper presented at the 21. In: CBECIMAT: Brazilian Congress of Engineering and Materials Science (Brazil).
Le-Bail, A., Maniglia, B.C., Le-Bail, P., 2020. Recent advances and future perspective in additive manufacturing of foods based on 3D printing. Curr. Opin. Food Sci. 35, 54–64. https://doi.org/10.1016/j.cofs.2020.01.009.
Lee, B.B., Ravindra, P., Chan, E.S., 2013. Size and shape of calcium alginate beads produced by extrusion dripping. Chem. Eng. Technol. 36 (10), 1627–1642. https://doi.org/10.1002/ceat.201300230.
Li, L., Fang, Y., Vreeker, R., Appelqvist, I., Mendes, E., 2007. Reexamining the egg-box model in calcium−alginate gels with X-ray diffraction. Biomacromolecules 8 (2), 464–468. https://doi.org/10.1021/bm060550a.
Li, Q., Duan, M., Hou, D., Chen, X., Shi, J., Zhou, W., 2021. Fabrication and characterization of Ca(II)-alginate-based beads combined with different polysaccharides as vehicles for delivery, release and storage of tea polyphenols. Food Hydrocolloids 112, 106274. https://doi.org/10.1016/j.foodhyd.2020.106274.
Lipton, J.I., Cutler, M., Nigl, F., Cohen, D., Lipson, H., 2015. Additive manufacturing for the food industry. Trends Food Sci. Technol. 43 (1), 114–123. https://doi.org/10.1016/j.tifs.2015.02.004.
Liu, Y., Tang, T., Duan, S., Qin, Z., Li, C., Zhang, Z., Wu, W., 2020. Effects of sodium alginate and rice variety on the physicochemical characteristics and 3D printing feasibility of rice paste. LWT 127, 109360. https://doi.org/10.1016/j.lwt.2020.109360.
Madziva, H., Kailasapathy, K., Phillips, M., 2005. Alginate–pectin microcapsules as a potential for folic acid delivery in foods. J. Microencapsul. 22 (4), 343–351. https://doi.org/10.1080/02652040500100931.
Makaremi, M., Yousefi, H., Cavallaro, G., Lazzara, G., Goh, C.B.S., Lee, S.M., Pasbakhsh, P., 2019. Safely dissolvable and healable active packaging films based on alginate and pectin. Polymers 11 (10), 1594. https://doi.org/10.3390/polym11101594.
Mishra, R.K., Datt, M., Banthia, A.K., 2008. Synthesis and characterization of pectin/PVP hydrogel membranes for drug delivery system. AAPS PharmSciTech 9 (2), 395–403. https://doi.org/10.1208/s12249-008-9048-6.
Moreira, H.R., Munarin, F., Gentilini, R., Visai, L., Granja, P.L., Tanzi, M.C., Petrini, P., 2014. Injectable pectin hydrogels produced by internal gelation: pH dependence of gelling and rheological properties. Carbohydr. Polym. 103, 339–347. https://doi.org/10.1016/j.carbpol.2013.12.057.
Nguyen, D., Hägg, D.A., Forsman, A., Ekholm, J., Nimkingratana, P., Brantsing, C., Simonsson, S., 2017. Cartilage tissue engineering by the 3D bioprinting of iPS cells in a nanocellulose/alginate bioink. Sci. Rep. 7 (1), 658. https://doi.org/10.1038/s41598-017-00690-y.
Periard, D., Schaal, N., Schaal, M., Malone, E., Lipson, H., 2007. Printing food. Paper presented at the. In: Proceedings of the 18th Solid Freeform Fabrication Symposium (Austin, TX).
Prasetyaningrum, A., Utomo, D.P., Raemas, A.F.A., Kusworo, T.D., Jos, B., Djaeni, M., 2021. Alginate/κ-carrageenan-based edible films incorporated with clove essential oil: physico-chemical characterization and antioxidant-antimicrobial activity. Polymers 13 (3). https://doi.org/10.3390/polym13030354.
Saarai, A., Kasparkova, V., Sedlacek, T., Saha, P., 2013. On the development and characterisation of crosslinked sodium alginate/gelatine hydrogels. J. Mech. Behav. Biomed. Mater. 18, 152–166. https://doi.org/10.1016/j.jmbbm.2012.11.010.
Schaffner, M., Rühs, P.A., Coulter, F., Kilcher, S., Studart, A.R., 2017. 3D printing of bacteria into functional complex materials. Sci. Adv. 3 (12), eaao6804 https://doi.org/10.1126/sciadv.aao6804.
Sokolovska, I., Kambulova, J., Overchuk, N., 2016. Study of the water binding in the gel systems of pectin and sodium alginate. E. Eur. J. Enterprise Technol. 2 (11), 4–11. https://doi.org/10.15587/1729-4061.2016.65746, 80.
Stachowiak, N., Kowalonek, J., Kozlowska, J., 2021. Freeze-dried matrices composed of degradable polymers with surfactant-loaded microparticles based on pectin and sodium alginate. Materials 14 (11). https://doi.org/10.3390/ma14113044.
Sun, J., Zhou, W., Huang, D., Fuh, J.Y.H., Hong, G.S., 2015. An overview of 3D printing technologies for food fabrication. Food Bioprocess Technol. 8 (8), 1605–1615. https://doi.org/10.1007/s11947-015-1528-6.
Tibbits, C.W., MacDougall, A.J., Ring, S.G., 1998. Calcium binding and swelling behaviour of a high methoxyl pectin gel. Carbohydr. Res. 310 (1), 101–107. https://doi.org/10.1016/S0008-6215(98)00172-4.
Ubeyitogullari, A., Ciftci, O.N., 2016. Formation of nanoporous aerogels from wheat starch. Carbohydr. Polym. 147, 125–132. https://doi.org/10.1016/j.carbpol.2016.03.086.
Vaziri, A.S., Alemzadeh, I., Vossoughi, M., Khorasani, A.C., 2018. Co-microencapsulation of Lactobacillus plantarum and DHA fatty acid in alginate-pectin-gelatin biocomposites. Carbohydr. Polym. 199, 266–275. https://doi.org/10.1016/j.carbpol.2018.07.002.
Vicini, S., Mauri, M., Wichert, J., Castellano, M., 2017. Alginate gelling process: use of bivalent ions rich microspheres. Polym. Eng. Sci. 57 (6), 531–536. https://doi.org/10.1002/pen.24552.
Walkenström, P., Kidman, S., Hermansson, A.-M., Rasmussen, P.B., Hoegh, L., 2003. Microstructure and rheological behaviour of alginate/pectin mixed gels. Food Hydrocolloids 17 (5), 593–603. https://doi.org/10.1016/S0268-005X(02)00119-4.

Yang, X., Nisar, T., Liang, D., Hou, Y., Sun, L., Guo, Y., 2018. Low methoxyl pectin gelation under alkaline conditions and its rheological properties: using NaOH as a pH regulator. Food Hydrocolloids 79, 560–571. https://doi.org/10.1016/j.foodhyd.2017.12.006.

Ye, H., Chen, T., Huang, M., Ren, G., Lei, Q., Fang, W., Xie, H., 2021. Exploration of the microstructure and rheological properties of sodium alginate-pectin-whey protein isolate stabilized B-carotene emulsions: to improve stability and achieve gastrointestinal sustained release. Foods 10 (9). https://doi.org/10.3390/foods10091991.

You, F., Wu, X., Chen, X., 2017. 3D printing of porous alginate/gelatin hydrogel scaffolds and their mechanical property characterization. International Journal of Polymeric Materials and Polymeric Biomaterials 66 (6), 299–306. https://doi.org/10.1080/00914037.2016.1201830.